A method of determining narrow energy spread electron beams from a laser plasma wakefield accelerator using undulator radiation

J. G. Gallacher,[1] M. P. Anania,[1] E. Brunetti,[1] F. Budde,[2,6] A. Debus,[2,5] B. Ersfeld,[1] K. Haupt,[2,3] M. R. Islam,[1] O. Jäckel,[2] S. Pfotenhauer,[2,7] A. J. W. Reitsma,[1] E. Rohwer,[3] H.-P. Schlenvoigt,[2,4] H. Schwoerer,[2,3] R. P. Shanks,[1] S. M. Wiggins,[1] and D. A. Jaroszynski[1,a)]

[1]*Department of Physics, Scottish Universities Physics Alliance, University of Strathclyde, Glasgow G4 0NG, United Kingdom*
[2]*Institut für Optik und Quantenelektronik, Friedrich-Schiller-Universität, 07743 Jena, Germany*
[3]*Laser Research Institute, University of Stellenbosch, 7602 Matieland, South Africa*
[4]*LULI-École Polytechnique, 91128 Palaiseau, France*
[5]*Forschungszentrum Dresden-Rossendorf, 01314 Dresden, Germany*
[6]*Institut für Laser-und Plasmaphysik, Heinrich-Heine-Universität Düsseldorf, 40225 Düsseldorf, Germany*
[7]*Massachusetts Institute of Technology, Cambridge, Massachusetts 02139, USA*

(Received 8 June 2009; accepted 11 August 2009; published online 2 September 2009)

In this paper a new method of determining the energy spread of a relativistic electron beam from a laser-driven plasma wakefield accelerator by measuring radiation from an undulator is presented. This could be used to determine the beam characteristics of multi-GeV accelerators where conventional spectrometers are very large and cumbersome. Simultaneous measurement of the energy spectra of electrons from the wakefield accelerator in the 55–70 MeV range and the radiation spectra in the wavelength range of 700–900 nm of synchrotron radiation emitted from a 50 period undulator confirm a narrow energy spread for electrons accelerated over the dephasing distance where beam loading leads to energy compression. Measured energy spreads of less than 1% indicates the potential of using a wakefield accelerator as a driver of future compact and brilliant ultrashort pulse synchrotron sources and free-electron lasers that require high peak brightness beams. © *2009 American Institute of Physics*. [doi:10.1063/1.3216549]

I. INTRODUCTION

Synchrotron sources have become ubiquitous tools for studying the structure of matter at the atomic and molecular length scale. These sources are among the largest scientific instruments in existence and are used by extensive industrial and academics communities from a wide range of research fields from physics, chemistry, engineering to the health sciences.[1] Conventional synchrotron sources are based on relativistic electron beams and deliver very high brightness pulses of electromagnetic radiation over a wide spectral range stretching from terahertz frequencies to hard x rays. The next "fourth generation light sources" are based on free-electron lasers (FELs) and provide coherent radiation with a peak brilliances which are many orders of magnitude higher than available from a synchrotron. Their potential as brilliant time resolved x-ray probes for taking femtosecond resolution "snapshots" of molecular and solid-state dynamics[1,2] makes them particularly attractive as large national and international facilities, such as those being constructed at the Linac Coherent Light Source (LCLS) in the United States,[3] the X-ray Free Electron Laser (XFEL) in Europe,[4] and the SPring-8 Compact Self-amplified spontaneous emission Source (SCSS) in Asia.[5]

Current light sources utilize rf accelerating structures to accelerate bunches of electrons to relativistic energies, which are then injected into magnetic structures, or insertion devices, to produce periodic transverse acceleration and electromagnetic radiation that can be tuned over a wide spectral range. Electrical breakdown in rf cavities currently limits the maximum sustainable electric field of conventional accelerators to less than 100 MV m^{-1}, which results in very large and expensive devices requiring large infrastructure and teams of engineers to service them. In addition, the pulse durations of synchrotrons are usually relatively long, of the order of 10 ps, which limits their usefulness as an ultrafast probe. The bunch duration can be reduced to less than 100 fs, but with a great deal of effort using magnetic compressors and/or electron bunch slicing techniques.[6]

A very attractive and compact alternative to rf acceleration is acceleration by plasma waves, a method that was first proposed in 1979 by Tajima and Dawson.[7] In these devices, a plasma density wake is driven either by the Coulomb force of a charged particle beam[8] or by the ponderomotive force of an intense ultrashort laser pulse, as in the laser wakefield accelerator (LWFA).[9] The wake forms a series of charge density structures with dimensions of the order of the plasma wavelength, $\lambda_p = 2\pi c/\omega_p$, which trail the laser pulse at approximately the group velocity, $[v_g \simeq c(1-n_e/n_c)^{1/2}]$, where ω_p is the plasma frequency, n_e is the plasma density, $n_c = m_e \varepsilon_0 \omega_0^2 / e^2$ is the critical density, ε_0 is the permittivity of free space, m_e is the electron mass, ω_0 is the laser frequency, and c is the speed of light in vacuum. These "accelerating cavity" structures due to charge separation produce an electric field that can be more than three orders of magnitude

a)Electronic mail: d.a.jaroszynski@strath.ac.uk.

greater than that found in rf accelerators, i.e., in excess of 100 GV m^{-1}.[10] The first demonstrations of controlled acceleration of quasimonoenergetic electron bunches from a LWFA were reported in 2004.[11–13] Since then, 1 GeV electron bunches have been produced in centimeter-long plasma capillary waveguide accelerating structures.[14,15]

With the availability of commercial multiterawatt laser systems based on chirped pulse amplification[16] there is a real prospect of accelerators based on plasma becoming widely used in university-sized establishments as drivers of radiation sources. Advantages of a wakefield based synchrotron light source include its high peak brilliance and ultrashort pulse duration, which is a fraction of a plasma oscillation period, $2\pi/\omega_p$, i.e., of the order of 10 fs for plasma densities $n_p \approx 10^{18}-10^{19}$ cm^{-3}.[17] Such a source would be very attractive for ultrafast x-ray probing studies.[1,2,18] Commercial terawatt lasers are currently limited to 10 Hz and there is excellent prospect for further development of lasers to increase their repetition rates to a kilohertz and above. This would increase the average brilliance. However, the real potential of a wakefield accelerator is as a compact driver of a FEL, because their electron beams have very high peak currents, small emittances and narrow energy spreads.

As a first step toward developing a LWFA based radiation source, narrow-bandwidth synchrotron radiation has been produced using an electron beam from a LWFA. In these experiments the wavelength scaling with beam energy[19] and the production of harmonics was demonstrated.[20] Here undulator radiation was produced by an electron beam from a LWFA and measurements confirmed the wavelength scaling with energy and thus the potential for a sub-10 fs duration x-ray synchrotron source.[19,20] However, to exceed the threshold for FEL action at x-ray photon energies, the major challenge is to produce a very high quality electron beam with a sufficiently high charge density, low emittance and small energy spread[2] to give net gain. rf accelerators can deliver such beams and are currently providing the basis for developing several large scale x-ray FEL facilities.[1,2] LWFAs are currently delivering electron beams that have promising characteristics, which are deduced from both measurements and simulations. The current state-of-the-art wakefield accelerator produces electron beams with a peak current of between 1 and 10 kA [deduced from the measured charge in the range of 10–100 pC and the predicted bunch duration of 10 fs)[11–14,21]] and an emittance of the order of 1π mm mrad.[22] However, the measured energy spread is currently a few percent because of the limited resolution of the electron energy spectrometers used in the studies.[11–14,21]

In this paper, we present measurements of the electron energy spectrum of a beam from a LWFA deduced from the spectrum of synchrotron radiation emitted from an undulator. We show that the total rms relative energy spread of a LWFA beam can be close to 1% and demonstrate a new method of determining the electron energy spread from the measured synchrotron radiation spectrum, which can be used at arbitrarily high electron beam energies. We also provide a theoretical explanation for the small observed energy spreads, which are smaller than predicted by previous simulations.[23,24] We compare the undulator spectrum deduced from the deconvoluted electron energy spectrum, taking into account the electron beam divergence and detector acceptance angle, and show that the optical and electron spectra are self-consistent. Our study demonstrates the viability of using an undulator as an electron energy spectrometer, which may be particularly useful at high energies (>1 GeV) where conventional high resolution magnetic dipole deflection spectrometers become very large and lose resolution. Furthermore, these measurements highlight the growing potential of a LWFA as an ultracompact source of intense, tunable electromagnetic radiation, which is readily scalable to x-ray wavelengths.

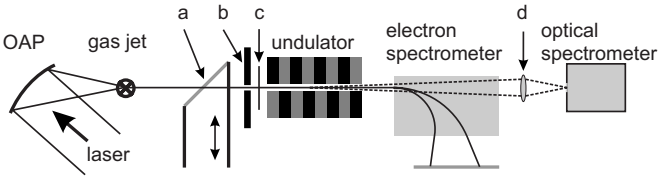

FIG. 1. Setup of the experiment. The laser pulse is focused by an OAP mirror into a supersonic helium gas jet where electrons are accelerated to between 50 and 70 MeV. The transverse electron beam profile is monitored on a removable scintillating screen. (a) A 1 cm thick, 1 cm inside diameter lead aperture (b) protects the undulator magnets from off-axis electrons. The spectrometer is shielded from direct laser and transition radiation exposure by a 15 μm thick aluminum foil (c) placed at the entrance of the undulator. The electrons traverse the undulator, produce synchrotron radiation, and are then dispersed in the magnetic electron spectrometer. Undulator radiation is collected by a lens (d) and analyzed by an optical spectrometer.

II. WAKEFIELD ACCELERATOR

The experiment to produce undulator synchrotron radiation using laser accelerated electrons has been carried out using the Jena Ti:sapphire (JETI) laser.[25] This laser delivers 85 fs duration laser pulses centered at a wavelength of 795 nm and with an energy of up to 430 mJ on target. The experimental setup is displayed in Fig. 1 and described in detail in Ref. 20. The laser pulses are focused by an $f/6$, 30° off-axis parabolic (OAP) mirror to a spot diameter of 11 μm at full-width at half-maximum (FWHM), yielding a peak intensity of 5×10^{18} W cm^{-2} and a normalized vector potential $a_0=1.5$. A pulsed supersonic helium gas jet, placed at the laser beam focus, produces a 2 mm diameter gas plume with a peak density of 2×10^{19} cm^{-3}. Nonlinear Thomson scattering from the plasma, at the second harmonic of the laser, is observed in the direction perpendicular to the laser polarization and is used to measure the length and position of the channel, as shown in Fig. 2. The electron beam divergence and pointing are observed on a removable Lanex scintillating screen[26,27] (Fig. 3) and optimized by moving the gas jet position, direction of the laser beam and tuning the gas density. This optimization procedure is also an essential step to steer the electron beam down the undulator axis. An example of an optimized transverse electron beam profile with a rms beam divergence of 2 mrad is shown in Fig. 3. This divergence is consistent with a normalized emittance of $\epsilon_n=1\pi$ mm mrad.

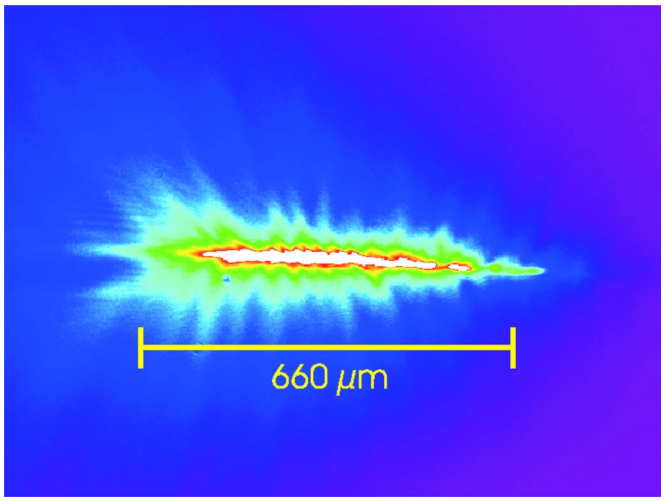

FIG. 2. (Color online) The relativistic plasma channel, self-illuminated at 2ω and used to characterize the length and position of the plasma channel.

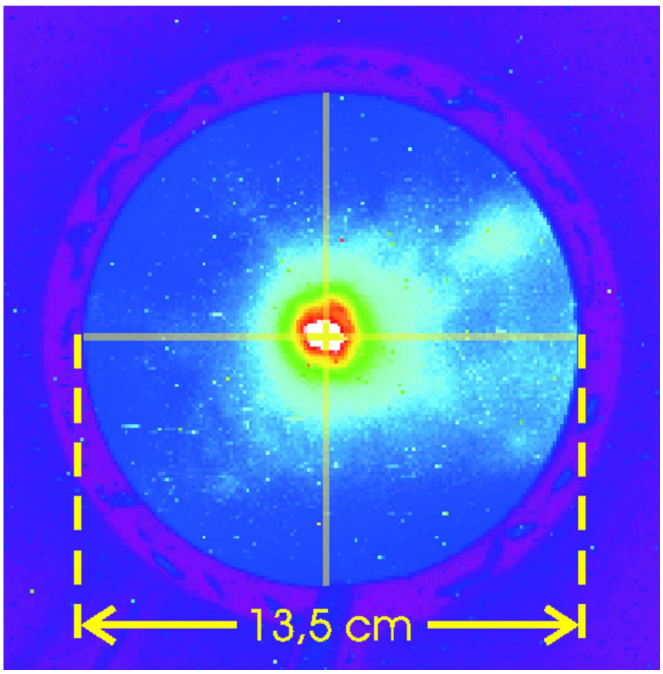

FIG. 3. (Color online) The transverse electron beam profile detected on the scintillating Lanex screen at the entrance of the undulator. Electron divergences in the range 2–10 mrad are observed. The shot displayed has a rms divergence of 2 mrad.

Following optimization of the electron beam properties, the scintillating screen is removed and the electrons are allowed to traverse the undulator, which is placed 40 cm downstream of the gas jet. A 50 period fixed-gap permanent magnet undulator, with wavelength $\lambda_u=2$ cm and pole gap of 10 mm, produces an on-axis peak magnetic field of $B_u=0.33$ T resulting in a deflection parameter $a_u=eB_u\lambda_u/2\pi m_0 c=0.6$. The undulator is placed in a vacuum chamber and has the fields of the initial and ultimate three periods carefully trimmed to ensure on-axis injection and exit of electrons. This shortens the undulator slightly, which marginally increases the homogeneous $(1/N_u)$ component of the undulator spectrum. A 1 cm thick, 1 cm diameter lead aperture [Fig. 1(b)] protects the undulator magnets from off-axis electron beams.

After traversing the undulator electrons are deflected by the magnetic field of an electron spectrometer (constructed from 200×100 mm^2 permanent magnets, separated by a 20 mm gap, giving a central magnetic field strength 0.72 T) placed 185 cm downstream of the gas jet. A scintillating screen (Lanex, Konica KR) and a charge-coupled device (CCD) camera detect the deflected electrons over an energy range of 14–85 MeV. The scintillation screen intensity has been calibrated using an imaging plate (Fuji BAS—MS2025) to give an absolute measure of the charge per unit energy.[27] This takes into account both the response of the image plate and the scintillating screen.

Undulator radiation is collected within a collection angle of 3 mrad and focused onto the entrance slit plane of a symmetric 200 mm Czerny–Turner spectrometer with a 105 mm focal length fused silica lens. A thermoelectrically cooled CCD camera (Andor DO-420 BN) is used to measure the spectrum of the undulator radiation. The CCD chip (1024×256 pixels) is operated in a hardware binning mode, by merging 8×12 pixels arrays into superpixels. The spectral range is set to 540–990 nm and the spectrometer and detector efficiency carefully calibrated using a standard visible-light source. The optical spectrometer is shielded against direct exposure from the laser and plasma light by a 15 μm thick aluminum foil placed in front of the undulator.

The maximum electron energy from a wakefield acceleration is fixed by the plasma density, which sets the length over which the accelerating electron beam outruns the plasma density wake. Because the plasma wake bubblelike structure travels at a velocity close to the group velocity of the laser pulse v_g and electrons in the wake are quickly accelerated to a velocity very close to the speed of light $v\simeq c$, then the difference between the wake and electron velocities implies that electrons traverse half a relativistic plasma wake wave λ_p over a length $L_d=c\omega_0^2/\omega_p^3$. When $a_0>1$, as it is in the experiments described here, electrons driven by the laser become relativistic and the bubble structure elongates and widens. Thus the dephasing length increases to $L_d=(4/3)\times(\omega_0^2/\omega_p^3)c\sqrt{a_0}$.[28] The plasma density in the region of the gas jet where electrons are accelerated is $n_e\approx1\times10^{19}$ cm^{-3}, which gives a relativistic plasma wavelength of 12.8 μm for $a_0=1.5$, thus $L_d\approx0.48$ mm, which is closely matched to the length of the gas jet used in the experiment. The maximum energy an electron can gain can be estimated by integrating the electric field over the dephasing length. The electric field amplitude inside the bubble is $E_0=\sqrt{a_0}mc\omega_p/e$,[28] thus the maximum energy an electron can gain from a plasma wave is

$$\gamma_{\max}=\frac{2}{3}\left(\frac{\omega_0^2}{\omega_p^2}\right)a_0. \tag{1}$$

Thus taking the plasma density in our experiment $(1\times10^{19}$ cm$^{-3})$, we can estimate an upper limit on the maximum energy an electron can gain to be ~178 MeV.

III. UNDULATOR RADIATION MEASUREMENTS

Linearly polarized undulator radiation is produced by the periodic transverse acceleration imparted to the electrons by the Lorentz force of the magnetic field of the undulator. The main spectral characteristics of the undulator radiation can be modeled using the well known undulator equation

$$\lambda = \frac{\lambda_u}{2h\gamma_z^2} = \frac{\lambda_u}{2h\gamma^2}\left(1 + \frac{a_u^2}{2} + \gamma^2\vartheta^2\right). \tag{2}$$

From this it can be seen that the peak wavelength emission depends on the undulator period λ_u and the electron energy $E_e = \gamma m_e c^2$, where γ is the Lorentz factor, h is the harmonic order, and ϑ is the angle with respect to the electron beam axis. The small reduction in the longitudinal velocity due to periodic deflection results in a slight increase in the wavelength of the emitted radiation by a factor $(1+a_u^2/2)$. The wavelength also exhibits an angular dependence through the $\gamma^2\vartheta^2$ term. The central radiation cone angular half width can be approximated as $\vartheta_{\text{cen}} = 1/\gamma\sqrt{N_u}$, which is approximately 1–1.3 mrad for the electron energies of the wakefield accelerator.

Given the known trajectory of an electron in the undulator, the radiation fields can be calculated by directly evaluating the retarded field of the Liénard–Wiechert potential.[29]

To help characterize the beam we consider the total brightness of the beam of radiation impinging on a surface as the power per unit area of the source from a unit solid angle. The brilliance, which is defined by $S_\omega = 2\epsilon_0 c|E|^2 \times$ area, is the power radiated (per unit frequency, beam area and solid angle) by a collimated electron beam of current density j_b. This is given by[30]

$$S_\omega(\omega,\vartheta) \approx \frac{k^2 L_u^2 e j_b}{32c\epsilon_0\pi^2\gamma^2}|A_u(\vartheta)|^2\left[\frac{\sin(\nu)}{\nu}\right]^2, \tag{3}$$

where ϑ is the angle between observation and motion directions and the normalized detuning parameter ν is given by

$$\nu = \pi N_u\left[\frac{\lambda_u}{2\lambda\gamma^2}\left(1 + \frac{a_u^2}{2} - \gamma^2\vartheta^2\right) - 1\right], \tag{4}$$

and the coefficient A_u is given by Ref. 30. Radiation over a spectral width $\delta\lambda_{\text{FWHM}}$ is emitted within an angle of approximately $\delta\vartheta_{\text{FWHM}}$. For angles less than $N_u^{1/2}\delta\vartheta_{FWHM}/2$, $A_u(\vartheta) \approx A_u(0)$ where

$$A_u(0) \approx a_u\left[J_0\left(\frac{a_u^2}{4+2a_u^2}\right) - J_1\left(\frac{a_u^2}{4+2a_u^2}\right)\right], \tag{5}$$

for the fundamental frequency. The spectrum consists of equally spaced odd harmonics on axis and both even and odd harmonics off axis, for a planar undulator. The spectrum of each harmonic is a sinc function $(\sin\nu^2/\nu^2)$ giving a FWHM spectral width of

$$\frac{\delta\lambda_{\text{FWHM}}}{\lambda} \approx \frac{0.9}{N_u h}. \tag{6}$$

For a particular harmonic, the solid angle of radiation emitted into the first lobe is

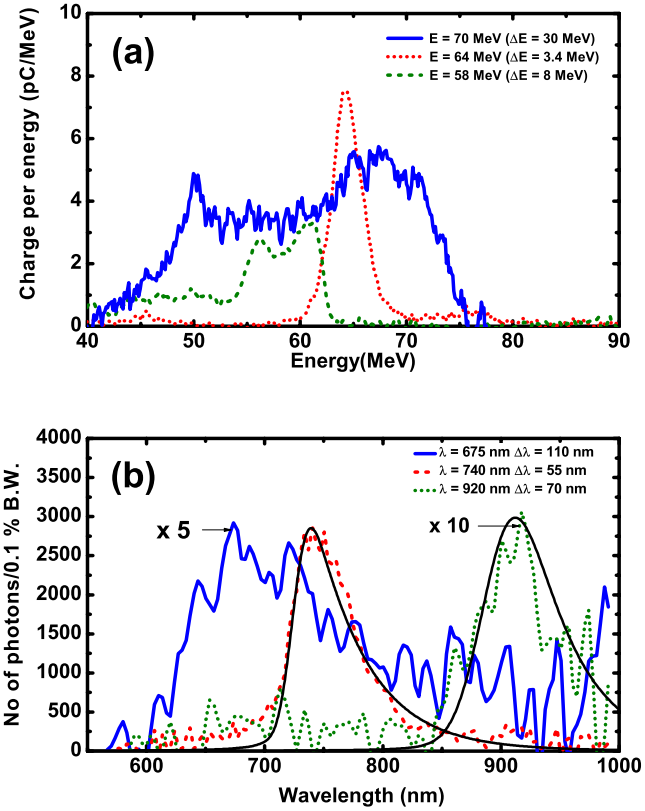

FIG. 4. (Color online) (a) The electron spectra and (b) the corresponding optical undulator radiation spectra for three shots. The blue (solid) and green (dotted) lines have been multiplied by 5 and 10, respectively for clarity. The black (solid) lines show the predicted spectra.

$$\delta\vartheta_{\text{FWHM}} \approx \frac{0.9}{(N_u h)^{1/2}} \cdot \frac{1 + a_u^2/2}{\gamma}, \tag{7}$$

with all harmonics emitted into the solid angle $\vartheta_{\text{FWHM}} \approx 1/\gamma_z = (1+a_u^2/2)^{1/2}/\gamma$ for an on-axis electron beam.

IV. UNDULATOR AS AN ELECTRON SPECTROMETER

To investigate the correspondence between the electron energy spectra and the undulator radiation spectra, several electron and optical spectra have been measured simultaneously. Figure 4 shows three representative pairs of measurements indicating the peak energy E, the FWHM spectral width, $\delta E/E$, the peak wavelength, λ, and the FWHM spectral bandwidth, $\delta\lambda/\lambda$. Consistent with Eq. (2), the wavelength decreases with increasing electron energy.[19] This characteristic scaling is clearly observed for both the fundamental $(h=1)$ and second harmonic $(h=2)$ emission.[20] Due to the limited spectral range of the optical spectrometer system, the fundamental and second harmonic signals could not be observed simultaneously. The measured radiation spectrum agrees well with predictions using Eq. (2) and numerical simulations[31] shown in Fig. 4(b) for wavelengths between 740 and 920 nm.

Undulator radiation provides a "signature" or "fingerprint" of the transverse and longitudinal electron beam characteristics. Thus, analysis of the undulator radiation spectra provides an attractive alternative method of characterizing

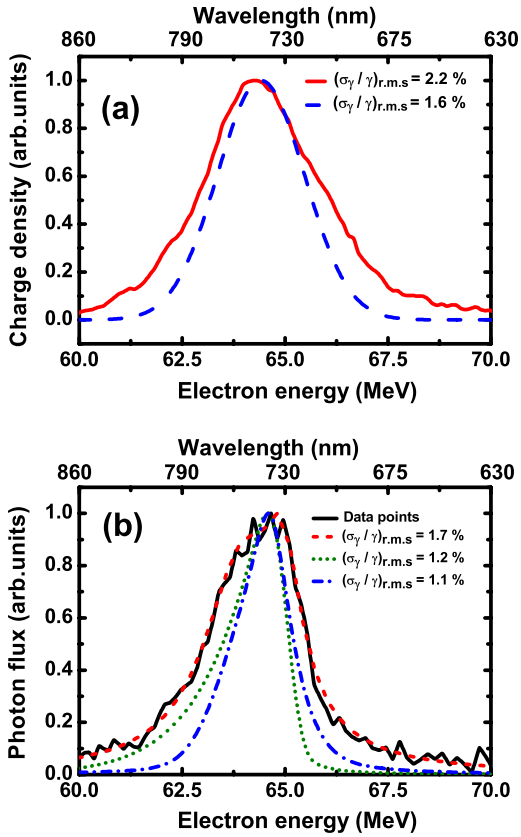

FIG. 5. (Color online) (a) The electron spectra data points (red solid line). The simulated instrument response function of the electron spectrometer, σ_γ/γ=1.6% (blue dashed line). (b) The undulator radiation spectra data points (black solid line). A best-fit curve to the data points, σ_γ/γ=1.7% (red dashed line). The simulated instrument response function of the magnetic undulator, σ_γ/γ=1.2% (green dotted line). The deconvoluted undulator spectrum, σ_γ/γ=1.1% (blue dash-dotted line). Note: The upper and lower axes in these plots give the respective wavelength and energy [Eq. (2)].

the electron beam properties with high resolution, compared with using a conventional magnetic spectrometer, particularly at high electron energies. To demonstrate this technique, an analysis of the experimental spectra shown in Fig. 4, corresponding to E=64 MeV, ΔE=3.4 MeV, λ=740 nm, and $\Delta\lambda$=55 nm, will be presented. These are replotted in Fig. 5 (red lines) for clarity. The corresponding measured FWHM widths of the electron spectra vary between 5.3% and 15% (σ_γ/γ in the range of 2.2%–6.2%).

The finite divergence and energy spread of the electron beam reduces the brilliance of the beam and smears out the spectrum as

$$S_\omega(\omega,\vartheta)=\int S_0(\omega,\gamma,\vartheta-\vartheta_e)F(\gamma,\vartheta_e)d\gamma d\vartheta_e, \tag{8}$$

where ϑ_e is the direction of electrons and S_0 is the distribution for a perfect beam with $\delta\gamma$=0 and $\delta\vartheta$=0.[32] $F(\gamma,\vartheta_e)$ is the energy and angular probability distribution of the beam. The total spectral width of the radiation is the sum of contributions from broadening due to the energy, angular, and natural spread components

$$\left(\frac{\delta\lambda}{\lambda}\right)^2=\left(\frac{2\sigma_\gamma}{\gamma}\right)^2+(\vartheta^2\gamma^2)^2+\frac{1}{N_u^2}. \tag{9}$$

To minimize the spectral width and thus maximize the brilliance, the second term, $(\vartheta^2\gamma^2)^2$, can be reduced by matching the electron beam to the undulator, which minimizes the beam divergence ϑ. To minimize the divergence the betatron wavelength, λ_β, which is analogous to the Rayleigh range of a laser beam, should be made approximately equal to the undulator length.[33] The rms emittance is defined as the transverse momentum/position phase-space area of the beam[33]

$$\epsilon_{\rm rms}=\langle x^2\rangle\left(\left\langle\left(\frac{p_x}{m_ec}\right)^2\right\rangle-\left\langle\frac{xp_x}{m_ec}\right\rangle^2\right)^{1/2}, \tag{10}$$

where p_x and x are the transverse momenta and coordinates of an electron, respectively. The edge or envelope emittance is four times as large. The un-normalized rms emittance $\epsilon_{\rm rms}$ of an electron beam of radius r_e is analogous to the wavelength of a laser beam (i.e., has units of length) and is given by

$$\epsilon_{\rm rms}=\pi\sigma_{\beta_\perp}r_e=k_\beta r_e^2, \tag{11}$$

where $\sigma_{\beta_\perp}$ is the variance of the (normalized) transverse velocities and $k_\beta=2\pi/\lambda_\beta=a_uk_u/2\gamma$ is the betatron wave number. The normalized emittance, $\epsilon_n=\beta_z\gamma\epsilon_{\rm rms}$ governs the broadening through $\gamma\vartheta$. The minimum beam divergence that is consistent with the smallest average beam radius gives $\lambda_\beta\approx L_u$, which occurs when the Fresnel number $F=r_e^2/\lambda L_u\approx 1$ and the electron beam divergence (given by $\vartheta\approx\epsilon_{\rm rms}/r_e$) matches the diffraction angle of radiation emitted by the undulator ($\vartheta\approx\lambda/r_e$), i.e., when

$$\vartheta^2=2k_\beta\epsilon_{\rm rms}, \tag{12}$$

and the brilliance is maximized, which is approximately 0.4 mrad for our parameters and a matched beam. However, in this case the electron beam was not focused into the undulator. Thus the dominant broadening contribution comes from the divergence of the beam, $\vartheta^2\gamma^2\approx 6\%$ corresponding to the beam divergence of approximately 2 mrad. The natural width is $1/N_u$=2.3%, taking into account the alteration of the first and last three periods for electron injection and exit. For the spectrum of Fig. 5(b), $(\delta\lambda/\lambda)_{\rm FWHM\ measured}$=7.4%, which gives an initial upper limit of 7.0% on the combined contributions from energy and angular spreads. The electron energy spectral width σ_γ/γ is limited to below 1.8%, which is smaller than the value of 2.4% obtained directly from the measured electron energy spectrum [red line in Fig. 5(a)].

To evaluate the actual electron beam energy spread, the measured spectra can be deconvoluted from the measured spectrum using the respective instrument response functions. This has been carried out for both the electron energy spectrum [Fig. 5(a)] and the undulator radiation spectrum [Fig. 5(b)]. In each case, the deconvoluted spectrum $\mathcal{S}_T$ is given by

$$\mathcal{S}_T=\mathcal{F}^{-1}\left(\frac{\mathcal{F}(\mathcal{C}_T)}{\mathcal{F}(\mathcal{R}_T)}\right), \tag{13}$$

where $\mathcal{F}$ denotes the Fourier transform, $\mathcal{C}_T$ is the convoluted measured spectrum, and $\mathcal{R}_T$ is the instrument response func-

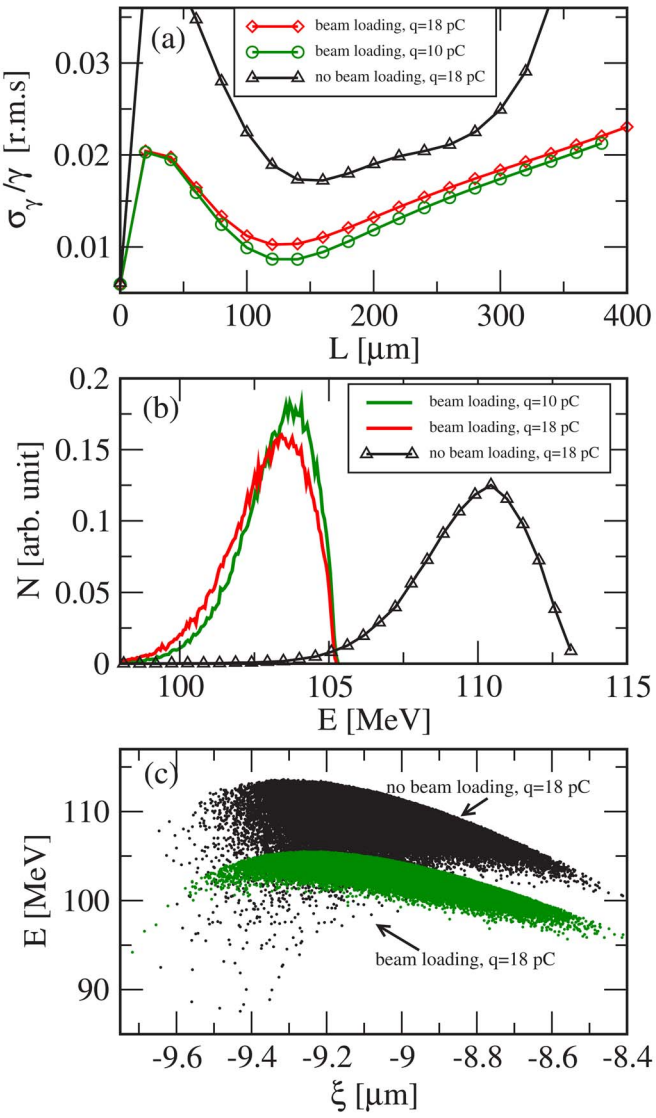

FIG. 6. (Color online) (a) Shows the spatial distribution of Lorentz factor of electrons at dephasing length (triangles for no beam loading, red (lower line) and green (upper line) for beam loading with 18 and 10 pC of charge, respectively), and (b) spectrum. Here (c) shows the energy compression as a function of propagation distance; triangle for no beam loading, square for beam loading when electron bunch charge is 18 pC (circle and triangle for beam loading when the bunch charge is 10 and 18 pC, respectively).

tion. The instrument response function for the electron spectrometer has been simulated using the general particle tracer (GPT) code[34] and is illustrated in Fig. 5(a) by the blue line. The equivalent σ_γ/γ for the spectrometer is 1.6%. This simulation takes into account all the relevant electron beam parameters and space charge effects.

For the corresponding radiation spectrum, the instrument response function of the undulator has been estimated using the three contributions to the measured spectral width of Eq. (9) such that

$$\mathcal{R}_T = \mathcal{F}^{-1}[\mathcal{F}(r_N) * \mathcal{F}(r_\theta) * \mathcal{F}(r_\gamma)], \tag{14}$$

where r_N, r_θ, and r_γ are the response functions due to natural broadening, angular spread and energy spread, respectively, which means that this response function refers back to the beam energy spread. However, as discussed above, the dominating term is due to the angular spread and so the overall undulator response function is presented in Fig. 5(b) by the green line (the corresponding σ_γ/γ is 1.2%). The deconvoluted spectrum [blue line in Fig. 5(b)]; therefore provides a final spectral width of $\sigma_\gamma/\gamma=1.2\%$. As a final check on the validity of this technique, this deconvoluted undulator spectrum has been convoluted with the electron spectrometer response function which gives a spectral width of 2.3% which is very close to the measured width of 2.2%. This confirms that the actual electron energy spread is close to 1%. The analysis has also been carried out for other experimental data shots with good agreement obtained between the measured and reconstructed spectra.

This method demonstrates the use of an undulator as a high resolution compact electron spectrometer of arbitrary resolution where the resolution depends on the number of undulator periods. At high electron energies an undulator is a very compact non-intercepting on-line alternative to very large magnetic dipole electron spectrometers.

The energy spread is reduced when the electrons are close to the dephasing length $L_d \approx \lambda_p \gamma_\phi^2/\pi$, i.e., when the electron beam reaches its maximum energy $\gamma \approx 2(\lambda_p/\lambda_0)^2$, where $\gamma_\phi=\lambda_p/\lambda_0$ is the Lorentz factor associated with the group velocity of the laser. Insight into the generation of narrow energy spread beams is gained from laser wakefield simulations. These have been carried out using a self-consistent reduced model that includes modifications of the laser pulse due to the local spatiotemporal refractive index modifications due to the plasma density variations of the wake.[23] To simulate self-injection, the electron bunch is injected at an optimal position into the wake behind the laser pulse. The bunch has a random initial phase-space distribution, determined by the energy spread and emittance. The model is implemented in a two-dimensional slab geometry, where both the laser pulse and the electron bunch are treated as collections of macroparticles of finite size. The evolution of the laser pulse $a(r,t)$ is calculated on a spatial grid, on which the macroparticles are treated classically by solving the classical equations of motion for the coupled dynamics of laser pulse, wakefield, and electron bunch. This correctly models "beam loading" which modifies the wakefield created by the laser pulse. As an initial condition we have considered a bunch occupying a volume of about 1 μm^3, and a laser potential of $a_0=2$ with a spot size of 10 μm, plasma density $n_0=1.2\times10^{19}$ cm^{-3}, and an electron bunch charge 10 and 18 pC, as shown in Fig. 6.

We observe lower energy spread for the beam loaded case ($<2\%$) because the electron bunch is accelerated by a uniform electrostatic field due to flattening of the potential. Without beam loading, the leading part of the electron bunch experiences a weaker acceleration field than the trailing part, which leads to a larger energy spread as observed in the simulations.

V. APPLICATION OF THE LWFA AS A DRIVER OF A RADIATION SOURCE

FELs require high brightness electron beams for high gain operation. This condition is met when the relative energy spread is less than the gain parameter, i.e., $\sigma_\gamma/\gamma < \rho$,[35] where ρ is the Pierce or FEL gain parameter, which also determines the efficiency,

$$\rho = \frac{1}{2\gamma}\left[\frac{I_p}{I_A}\left(\frac{\lambda_u a_u}{2\pi\sigma_x}\right)^2\right]^{1/3}, \tag{15}$$

where I_p is the peak electron beam current, $I_A = 4\pi\epsilon_0 m_e c^3/e \sim 17$ kA, the Alfven-current and σ_x is the beam diameter. The ideal gain length[35,36] is

$$L_g = \frac{\lambda_u}{4\pi\sqrt{3}\rho}. \tag{16}$$

In the presence of energy spread, emittance and diffraction, the L_g is increased by $(\Lambda+1)$ to $L_g = L_{\text{gain}*}(1+\Lambda)$.[36] To reduce the gain length and undulator length, ρ should be maximized. This is usually achieved by reducing the beam size, which requires extremely low emittances. However, as can be seen from Eqs. (15) and (16), the gain length may also be reduced by increasing the peak current. As electron bunches from wakefield accelerators are of the order of 10 fs, much shorter than the plasma wavelength, and the charge of the order of 100 pC, and the peak current can be very high (>10 kA), which is much higher than in rf accelerators. Hence, laser plasma-based electron accelerators may be ideal drivers for FELs. The next generation x-ray FELs are designed for relative energy spreads of 0.1% or less and low emittances $\epsilon_n \approx 1\pi$ mm mrad.[3,5] Up till now, the smallest energy spreads of LWFA electron bunches has been of the order of 2.5%.[11–15,21,37] Our measurement of energy spread $\approx 1\%$ is comparable to recent reports[38–40] and represents a very important step.

Ultrahigh beam currents are subject to strong space charge forces. When the electron bunch leaves the plasma and into vacuum, it begins to expand due to space charge forces. This can result in transverse space-charge expansion and longitudinal debunching.[41] However, space charge explosion may contribute to the energy spread for lower energies. Simulations that have been carried out using GPT (Ref. 34) show that space charge only has a very minor impact on the transverse and longitudinal emittances. This improves at higher electron energies, where space charge effects are much weaker; hence higher quality electron beams are produced.

As an example, consider a 1 GeV laser-produced electron beam[14] as a driver of the advanced laser-plasma high-energy accelerators toward x rays (ALPHA-X) undulator[42] ($\lambda_u = 1.5$ cm, $N_u = 200$, $a_u = 0.7$). This would lead to 2.5 nm wavelength, ultrashort, incoherent radiation pulses with a peak brilliance of $B \sim 10^{23}$ photons/s mrad^2 mm^2 0.1% bandwidth. Direct generation of coherent undulator radiation is more challenging as it requires electron bunches shorter than the emitted wavelength. Coherent emission from a prebunched beam will lead to infrared and far infrared radiation. However, to reach the ultraviolet or x-ray spectral region one must rely on the self-amplified spontaneous emission (SASE) mechanism. This involves microbunching of the electron beam with a wavelength periodicity due to the combined action of the laser beam with the undulator field. The initial field in SASE is synchrotron radiation, which results in amplified noise. However, an external source such as high order harmonics from a laser driven rare gas is also used as a seed.

VI. CONCLUSION

Using the demonstration of the first all optically driven undulator radiation source, we have illustrated how the undulator radiation spectrum is a signature of the electron beam energy distribution. This technique will apply to electrons of arbitrarily high energy and therefore will be of crucial importance in the diagnosis of future multi-GeV electron beams that cannot be precisely interrogated by magnetic dipole spectrometers. Analysis of the radiation spectrum allows the actual electron beam energy spread to be deduced which, in this case, was close to 1% accounting for the spectrometer response. Production of such a high quality beam is an important step toward the use of laser wakefield accelerators as drivers of synchrotron and FEL sources which require high electron peak current, low energy spread and low emittance. Extension of this experiment into the ultraviolet and x-ray wavelength regime and eventual coherent emission (SASE) of light will be an invaluable tool. The use of plasma undulators are also being investigated to shorten the undulator period.[43,44] This not only allows the use of lower energy electrons to reach vacuum ultraviolet wavelengths, but because of the high peak current, also shows promise as future compact coherent x-ray sources.

ACKNOWLEDGMENTS

This work was supported by the Deutsche Forschungsgemeinschaft under Contract No. TR18. Financial support by the Access to Research Infrastructures activity in the Sixth Framework Programme of the EU (Contract No. RII3-CT-2003-506350, Laserlab Europe) for conducting the research is gratefully acknowledged. We thank B. Beleites, F. Ronneberger, and W. Ziegler for their technical support. S.M.W. acknowledges the support of the Department of Physics, Lancaster University, and the Cockcroft Institute, Daresbury Laboratory, Daresbury, United Kingdom. The UK team also acknowledges the support of the Research Councils UK and the EU EuroLEAP NEST Contract No. 028514.

[1] D. H. Bilderback, P. Elleaume, and E. Weckert, J. Phys. B **38**, S773 (2005).
[2] J. Feldhaus, J. Arthur, and J. B. Hastings, J. Phys. B **38**, S799 (2005).
[3] P. H. Bucksbaum, AIP Conf. Proc. **926**, 3 (2007).
[4] G. Grübel, G. B. Stephenson, C. Gutt, H. Sinn, and Th. Tschentscher, Nucl. Instrum. Methods Phys. Res. B **262**, 357 (2007).
[5] T. Shintake, T. Tanaka, T. Hara, K. Togawa, T. Inagaki, Y. J. Kim, T. Ishikawa, H. Kitamura, H. Baba, H. Matsumoto, S. Takeda, M. Yoshida, and Y. Takasu, Nucl. Instrum. Methods Phys. Res. A **507**, 382 (2003).
[6] S. Khan, K. Holldack, T. Kachel, R. Mitzner, and T. Quast, Phys. Rev. Lett. **97**, 074801 (2006).
[7] T. Tajima and J. M. Dawson, Phys. Rev. Lett. **43**, 267 (1979).

[8]I. Blumenfeld, C. E. Clayton, F.-J. Decker, M. J. Hogan, C. Huang, R. Ischebeck, R. Iverson, C. Joshi, T. Katsouleas, N. Kirby, W. Lu, K. A. Marsh, W. B. Mori, P. Muggli, E. Oz, R. H. Siemann, D. Walz, and M. Zhou, Nature (London) **445**, 741 (2007).
[9]T. Katsouleas, Nature (London) **431**, 515 (2004).
[10]E. Esarey, P. Sprangle, J. Krall, and A. Ting, IEEE Trans. Plasma Sci. **24**, 252 (1996).
[11]S. P. D. Mangles, C. D. Murphy, Z. Najmudin, A. G. R. Thomas, J. L. Collier, A. E. Dangor, E. J. Divall, P. S. Foster, J. G. Gallacher, C. J. Hooker, D. A. Jaroszynski, A. J. Langley, W. B. Mori, P. A. Norreys, F. S. Tsung, R. Viskup, B. R. Walton, and K. Krushelnick, Nature (London) **431**, 535 (2004).
[12]C. G. R. Geddes, Cs. Toth, J. van Tilborg, E. Esarey, C. B. Schroeder, D. Bruhwiler, C. Nieter, J. Cary, and W. P. Leemans, Nature (London) **431**, 538 (2004).
[13]J. Faure, Y. Glinec, A. Pukhov, S. Kiselev, S. Gordienko, E. Lefebvre, J.-P. Rousseau, F. Burgy, and V. Malka, Nature (London) **431**, 541 (2004).
[14]W. P. Leemans, B. Nagler, A. J. Gonsalves, Cs. Toth, K. Nakamura, C. G. R. Geddes, E. Esarey, C. B. Schroeder, and S. M. Hooker, Nat. Phys. **2**, 696 (2006).
[15]K. Nakamura, B. Nagler, Cs. Toth, C. G. R. Geddes, C. B. Schroeder, E. Esarey, and W. P. Leemans, Phys. Plasmas **14**, 056708 (2007).
[16]P. Maine, D. Strickland, P. Bado, M. Pessot, and G. Mourou, IEEE J. Quantum Electron. **24**, 398 (1988).
[17]A. Pukhov and J. Meyer-ter-Vehn, Appl. Phys. B: Lasers Opt. **74**, 355 (2002).
[18]K. Sokolowski-Tinten and D. von der Linde, J. Phys.: Condens. Matter **16**, R1517 (2004).
[19]H.-P. Schlenvoigt, K. Haupt, A. Debus, F. Budde, O. Jäckel, S. Pfotenhauer, H. Schwoerer, E. Rohwer, J. G. Gallacher, E. Brunetti, R. P. Shanks, S. M. Wiggins, and D. A. Jaroszynski, Nat. Phys. **4**, 130 (2008).
[20]H.-P. Schlenvoigt, K. Haupt, A. Debus, F. Budde, O. Jäckel, S. Pfotenhauer, J. G. Gallacher, E. Brunetti, R. P. Shanks, S. M. Wiggins, D. A. Jaroszynski, E. Rohwer, and H. Schwoerer, IEEE Trans. Plasma Sci. **36**, 1773 (2008).
[21]S. P. D. Mangles, A. G. R. Thomas, M. C. Kaluza, O. Lundh, F. Lindau, A. Persson, F. S. Tsung, Z. Najmudin, W. B. Mori, C.-G. Wahlström, and K. Krushelnick, Phys. Rev. Lett. **96**, 215001 (2006).
[22]S. Fritzler, E. Lefebvre, V. Malka, F. Burgy, A. E. Dangor, K. Krushelnick, S. P. D. Mangles, Z. Najmudin, J.-P. Rousseau, and B. Walton, Phys. Rev. Lett. **92**, 165006 (2004).
[23]A. J. W. Reitsma, R. A. Cairns, R. Bingham, and D. A. Jaroszynski, Phys. Rev. Lett. **94**, 085004 (2005).
[24]A. Reitsma, R. Trines, and V. Goloviznin, IEEE Trans. Plasma Sci. **28**, 1165 (2000).
[25]Jena laser specifications, http://www.physik.uni-jena.de/qe/technik/labor-1.html.
[26]Y. Glinec, J. Faure, A. Guemnie-Tafo, V. Malka, H. Monard, J. P. Larbre, V. De Waele, J. L. Marignier, and M. Mostafavi, Rev. Sci. Instrum. **77**, 103301 (2006).
[27]K. A. Tanaka, T. Yabuuchi, T. Sato, R. Kodama, Y. Kitagawa, and T. Takahashi, Rev. Sci. Instrum. **76**, 013507 (2005).
[28]W. Lu, M. Tzoufras, C. Joshi, F. S. Tsung, W. B. Mori, J. Vieira, R. A. Fonseca, and L. O. Silva, Phys. Rev. ST Accel. Beams **10**, 061301 (2007).
[29]J. D. Jackson, *Classical Electrodynamics*, 3rd ed. (Wiley, New York, 1999).
[30]P. Luchini and H. Motz, *Undulators and Free-Electron Lasers* (Clarendon, Oxford, 1990).
[31]T. Tanaka and H. Kitamura, J. Synchrotron Radiat. **8**, 1221 (2001).
[32]D. Attwood, *Soft X-Rays and Extreme Ultraviolet Radiation* (Cambridge University Press, New York, 1999).
[33]J. D. Lawson, *The Physics of Charged Particle Beams* (Oxford University Press, London, 1988).
[34]S. B. van der Geer, O. J. Luiten, M. J. de Loos, G. Pöplau, and U. van Rienen, *3D Space-Charge Model for GPT Simulations of High Brightness Electron Bunches*, Institute of Physics Conference Series No. 175 (IOP, Bristol, 2005), p. 101.
[35]R. Bonifacio, C. Pellegrini, and L. M. Narducci, Opt. Commun. **50**, 373 (1984).
[36]M. Xie, Nucl. Instrum. Methods Phys. Res. A **445**, 59 (2000).
[37]B. Hidding, K.-U. Amthor, B. Liesfeld, H. Schwoerer, S. Karsch, M. Geissler, L. Veisz, K. Schmid, J. G. Gallacher, S. P. Jamison, D. A. Jaroszynski, G. Pretzler, and R. Sauerbrey, Phys. Rev. Lett. **96**, 105004 (2006).
[38]S. M. Wiggins, M. P. Anania, E. Brunetti, S. Cipiccia, B. Ersfeld, M. R. Islam, R. C. Issac, G. Raj, R. P. Shanks, G. Vieux, G. H. Welsh, W. A. Gillespie, A. M. MacLeod, M. W. Poole, and D. A. Jaroszynski, Proc. SPIE **7359**, 735914 (2009).
[39]V. Malka, J. Faure, C. Rechatin, A. Ben-Ismail, J. K. Lim, X. Davoine, and E. Lefebvre, Phys. Plasmas **16**, 056703 (2009).
[40]K. Schmid, L. Veisz, F. Tavella, S. Benavides, R. Tautz, D. Herrmann, A. Buck, B. Hidding, A. Marcinkevicius, U. Schramm, M. Geissler, J. Meyer-ter-Vehn, D. Habs, and F. Krausz, Phys. Rev. Lett. **102**, 124801 (2009).
[41]F. Grüner, S. Becker, U. Schramm, T. Eichner, M. Fuchs, R. Weingartner, D. Habs, J. Meyer-ter-Vehn, M. Geissler, M. Ferrario, L. Serafini, B. van der Geer, H. Backe, W. Lauth, and S. Reiche, Appl. Phys. B: Lasers Opt. **86**, 431 (2007).
[42]D. A. Jaroszynski, R. Bingham, E. Brunetti, B. Ersfeld, J. Gallacher, B. van der Geer, R. Issac, S. P. Jamison, D. Jones, M. de Loos, A. Lyachev, V. Pavlov, A. Reitsma, Y. Saveliev, G. Vieux, and S. M. Wiggins, Philos. Trans. R. Soc. London Ser. A **364**, 689 (2006).
[43]R. L. Williams, C. E. Clayton, C. Joshi, C. Fellow, and T. C. Katsouleas, IEEE Trans. Plasma Sci. **21**, 156 (1993).
[44]C. Joshi, T. Katsouleas, J. M. Dawson, Y. T. Yan, and J. M. Slater, IEEE J. Quantum Electron. **23**, 1571 (1987).